Cell

The RCK Domain of the KtrAB K^+ Transporter: Multiple Conformations of an Octameric Ring

Ronald A. Albright,[1] José-Luís Vazquez Ibar,[1] Chae Un Kim,[2] Sol M. Gruner,[2,3] and João Henrique Morais-Cabral[1,*]
[1] Department of Molecular Biophysics and Biochemistry, Yale University, 266 Whitney Avenue, New Haven, CT 06520, USA
[2] Cornell High Energy Synchrotron Source
[3] Physics Department
Cornell University, Ithaca, NY 14853, USA
*Contact: joao.cabral@yale.edu
DOI 10.1016/j.cell.2006.08.028

SUMMARY

The KtrAB ion transporter is a complex of the KtrB membrane protein and KtrA, an RCK domain. RCK domains regulate eukaryotic and prokaryotic membrane proteins involved in K^+ transport. Conflicting functional models have proposed two different oligomeric arrangements for RCK domains, tetramer versus octamer. Our results for the KtrAB RCK domain clearly show an octamer in solution and in the crystal. We determined the structure of this protein in three different octameric ring conformations that resemble the RCK-domain octamer observed in the MthK potassium channel but show striking differences in size and symmetry. We present experimental evidence for the association between one RCK octameric ring and two KtrB membrane proteins. These results provide insights into the quaternary organization of the KtrAB transporter and its mechanism of activation and show that the RCK-domain octameric ring model is generally applicable to other ion-transport systems.

INTRODUCTION

RCK (*r*egulating the *c*onductance of K^+) domains (Jiang et al., 2001) modulate the function of some eukaryotic and prokaryotic potassium channels, including the eukaryotic BK potassium channel and the prokaryotic *Methanothermobacter thermoautotrophicus* MthK potassium channel (Jiang et al., 2002a, 2002b; Kuo et al., 2005; Loukin et al., 2005). The importance of RCK domains was demonstrated by a sequence analysis of 270 prokaryotic genomes (Kuo et al., 2005; Loukin et al., 2005), which revealed that over half of the K^+ channels detected (127 out of 217) have RCK domains, making them by far the most common nonintegral membrane domains present in prokaryotic K^+ channels. RCK domains are also present in the prokaryotic potassium transporters KtrAB, Trk, and KefC (Durell et al., 1999; Munro et al., 1991; Tholema et al., 1999), which play pivotal roles in the uptake of K^+ into the cell (Epstein, 2003). RCK domains associated with these transporter proteins are sometimes referred as KTN (*K*$^+$ *t*ransport, *n*ucleotide-binding) domains since some show homology to dinucleotide-binding domains (Durell et al., 1999; Roosild et al., 2002; Schlosser et al., 1993). The prevalence of RCK domains in prokaryotic potassium channels, together with their role in the regulation of potassium transporters, shows that these domains are a focal point in the physiological regulation of K^+ homeostasis in prokaryotes. In all these protein systems, it is thought that binding of a specific ligand induces a conformational change in the RCK domain that is propagated to the membrane-bound protein, leading to ion transport (Jiang et al., 2002a; Roosild et al., 2002).

Structures have been determined for the RCK domains of *E. coli* Kch (Jiang et al., 2001) and *M. thermoautotrophicus* MthK (Dong et al., 2005; Jiang et al., 2002a, 2002b) potassium channels and the *B. subtilis* KtrAB and *Methanococcus jannaschii* Trk ion transporters (Roosild et al., 2002). The basic assembly in all these structures is a homodimer. Each dimer subunit has an N-terminal subdomain (~124 residues long) that adopts a Rossmann fold where a ligand binds, followed by a crossover helix (~13–17 residues) that intercalates into the partner subunit (see Figure 1) and a roughly 80 residue long C-terminal subdomain. The N-terminal subdomain exhibits some sequence conservation within RCK subfamilies. By contrast, the C-terminal region appears to be much more variable.

At present, there are two conflicting models for the functional oligomeric arrangement of RCK domains. The structure of the MthK potassium channel (Jiang et al., 2002a, 2002b) reveals an intriguing arrangement of eight RCK domains (a tetramer of dimers); in this structure, two tetrameric channels are stacked foot to foot through their tethered RCK domains. In the MthK channel, a Ca^{2+} binds

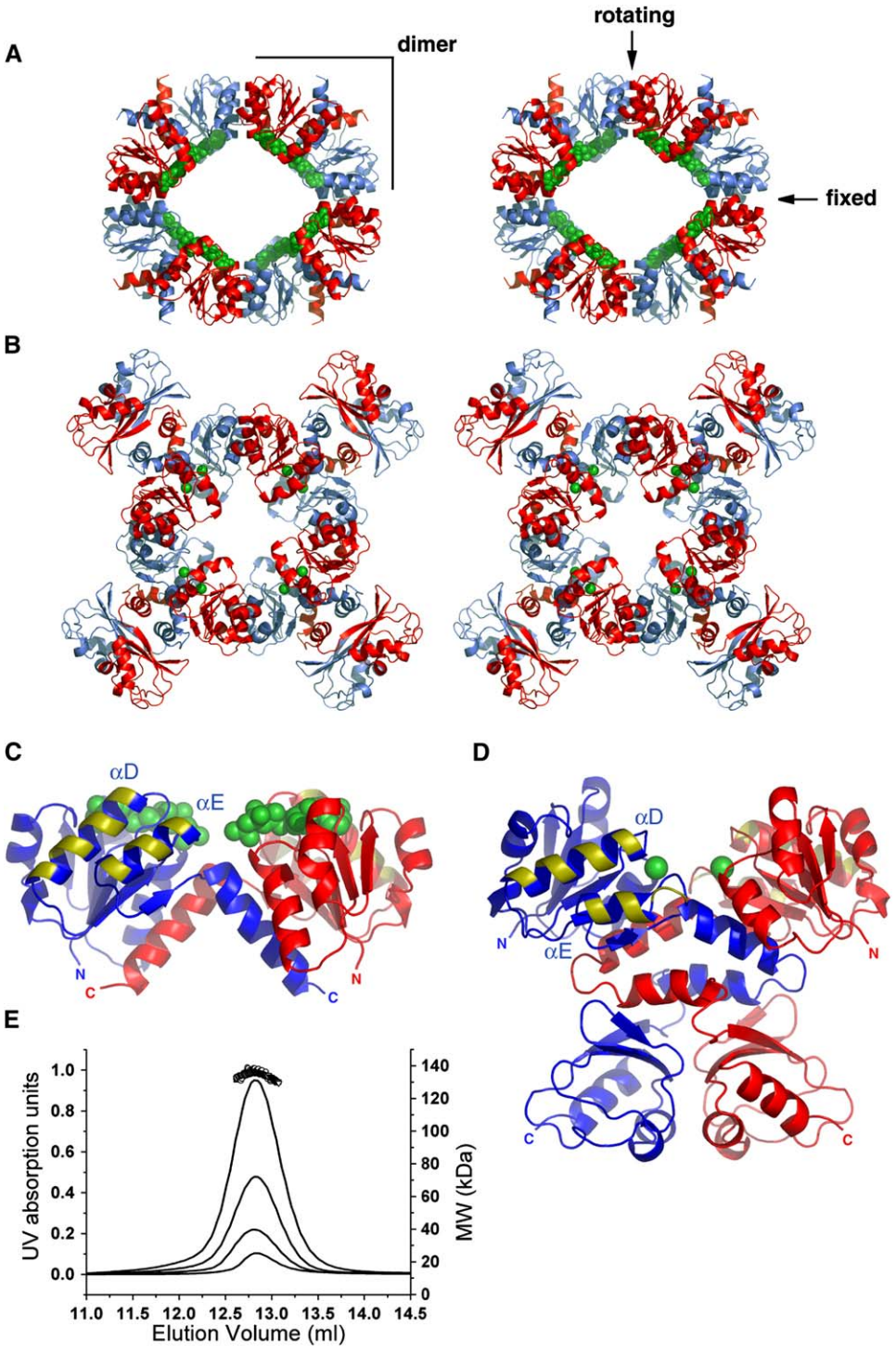

Figure 1. The Diamond Conformation

(A) Stereoview of the truncated KtrAB RCK-domain octameric ring. Alternating subunits are shown in red and blue; ordered parts of NADH ligands are shown as green spheres.

(B) Stereoview of the RCK-domain octameric ring from the MthK channel. Protein is shown in ribbon; calcium ions are shown as green spheres. (A) and (B) are on the same scale.

(C) Ribbon representation of KtrAB RCK-domain homodimer. Subunits are shown in different colors; ordered parts of NADH ligands are shown as green spheres. The dimer is oriented so that the top of the figure corresponds to the inside of the ring. Yellow shading on two of the helices (αD and αE) represents molecular surfaces involved in dimer-to-dimer interfaces.

within a cleft of each RCK domain not far from the dimer interface; functional studies have shown that Ca^{2+} binding increases the open probability of the channel. This structural information, together with biochemical data, led to a functional model where, in the cell, the MthK-channel RCK domains form an octameric ring on the cytoplasmic face of the channel with four domains tethered to the channel subunits and four other RCK domains existing as independent polypeptides. Gating (opening and closing) of the channel is proposed to result from RCK-ring expansion or contraction in response to a change, induced by calcium binding, in the relative positions of the subunits within the homodimer assembly (Jiang et al., 2002a). Recent biochemical data on isolated MthK RCK domains have provided additional support for this octameric arrangement (Dong et al., 2005).

The other oligomeric functional model is based on structural studies (Roosild et al., 2002) of the RCK domain from the KtrAB ion transporter. This transporter is a complex of the membrane-bound KtrB protein and the cytoplasmic KtrA protein, an RCK domain (Durell et al., 1999; Matsuda et al., 2004; Nakamura et al., 1998). The KtrB protein is thought to have eight transmembrane helices that adopt the structural architecture typical of the pore of a potassium channel (Durell et al., 1999; Tholema et al., 1999, 2005). The structure of a truncated form of the KtrA protein (with the variable C-terminal subdomain removed) was solved bound to NADH (Roosild et al., 2002). A comparison of the RCK domain structures of this transporter and of the MthK channel revealed the same homodimer assembly; the ligands, calcium ion in MthK and NADH in KtrAB, bind within the same groove of the N-terminal subdomain (Dong et al., 2005). The crystal structures of the truncated KtrA bound to NADH and of the related Trk RCK domain bound to NAD^+, together with solution studies (Roosild et al., 2002), formed the basis of an ion-transport activation model where four RCK domains (a dimer of dimers) bind to the membrane protein and regulate its function. It was proposed that, in response to ligand, there are changes in the RCK dimer organization that lead to the destabilization of the tetramer and inactivation of the transporter.

The two contrasting quaternary arrangements proposed for the RCK domains of KtrAB (Roosild et al., 2002) and MthK (Jiang et al., 2002a, 2002b) (tetramer versus octamer) are intriguing since both have at their basis a very similar homodimer assembly and both models propose ligand-induced changes in the relative orientation of the subunits across the dimer interface. It is also clear that both proposals have shortcomings: The tetrameric model is based on an artificially imposed remodeling of crystal lattice contacts of the structures from two different RCK domains, while the octameric ring proposal is based on a nonphysiological crystal structure where two channels are stacked foot to foot through their cytoplasmic domains. The contradictions of the two models together with the importance of RCK domains for the regulation of potassium-transport systems in prokaryotes and of channels in eukaryotes led us to revisit the structure of the RCK domain of KtrAB. Here we show that this protein adopts an oligomeric state that contrasts with the previous report: We reveal different conformations of the oligomer and provide experimental data supporting an unanticipated stoichiometry of the KtrAB complex. Together, these results unify our understanding of the molecular mechanism underlying ligand activation by the RCK domain family.

RESULTS

Ring Structure

The truncated RCK domain from the *B. subtilis* KtrAB ion transporter was cloned and expressed using published protocols (Roosild et al., 2002) with minor modifications. A search for new crystal forms produced crystals in the presence of NADH that diffract to 2.2 Å. We solved the structure (R_{work} 23.2.0%, R_{free} 25.8%) by molecular replacement using a single domain of the previously deposited KtrAB RCK coordinates (PDB ID code 1LSU) (Roosild et al., 2002) and found a homodimer in the asymmetric unit.

Surprisingly, analysis of the crystal lattice contacts showed the RCK domains organized as an octameric ring (Figure 1A). This quaternary arrangement with an up-and-down disposition of the subunits around the ring is similar to the one observed in the MthK structure (Figure 1B) (Jiang et al., 2002a, 2002b). The up-domains in the ring (colored red in the figure) do not directly contact each other, with interactions being mediated by intervening down-domains (blue). The KtrAB RCK ring takes the shape of a diamond with 222 point-group symmetry, with each homodimer defining a side of the diamond and the dimer interface at the center of the side (Figures 1A and 1B). Dimer-to-dimer interfaces are located at the corners of the diamond and come in two types that we refer to as rotating and fixed for reasons that will become clear.

As previously shown for MthK and KtrAB (Roosild et al., 2002), each RCK subunit consists of a Rossmann fold (Bellamacina, 1996; Jiang et al., 2001) followed by a crossover helix that extends over to its partner in the dimer (Figure 1C). The NADH ligands are bound at positions flanking the dimer interface and line the hole of the ring

(D) Ribbon representation of MthK RCK-domain homodimer. Yellow shading marks the regions involved in dimer-to-dimer interfaces. Calcium ions are shown as green spheres. The scale is the same as used in (C). All molecular representations were prepared with PyMOL (http://pymol.sourceforge.net/).

(E) Light-scattering measurements of the KtrAB RCK domain. The four continuous "bell-shaped" lines are the UV traces of protein eluting from the size-exclusion column at different dilutions. The points above the UV traces correspond to the determined solution molecular weight of the macromolecule at different points in the eluted protein peak.

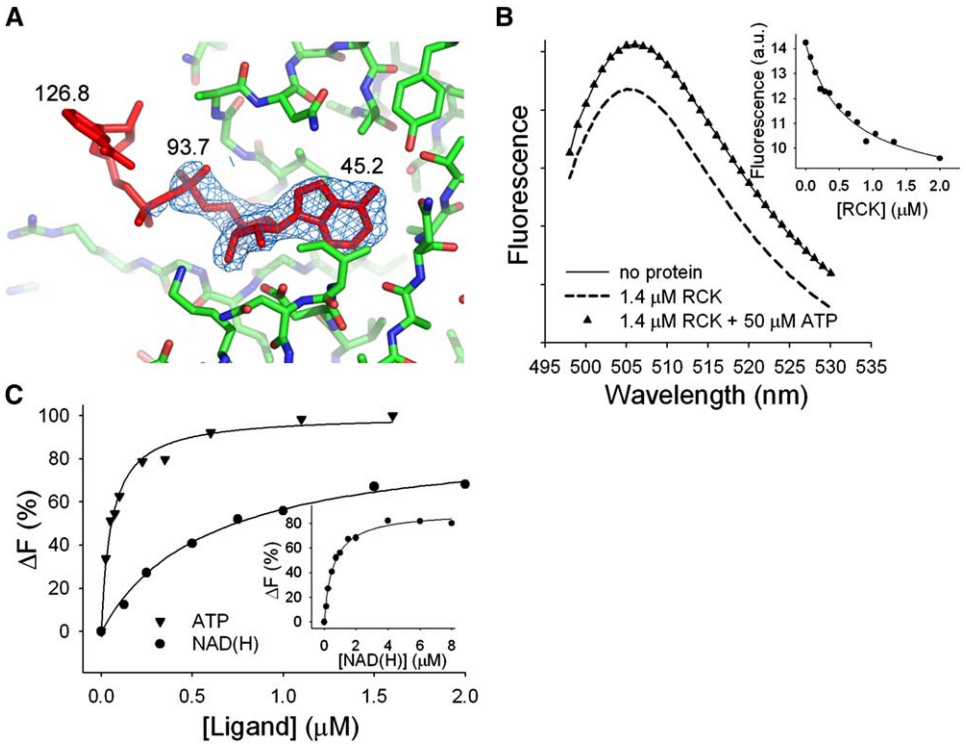

Figure 2. Ligand Studies

(A) Simulated annealing omit electron-density map of the NADH molecule (in red) in the diamond octamer ring contoured at 1 sigma. The average temperature-factor values of the adenine ring, the first phosphate, and the nicotinamide ring are shown. The average temperature factor of the binding pocket main chain is 41.6 Å^2.

(B) Examples of fluorescence spectra of ATP-γS-BODIPY alone, with protein, and with protein plus ATP. Inset shows a fit of a Langmuir isotherm (Equation 1) to the ATP-γS-BODIPY titration data.

(C) Examples of ATP and NADH competition experiments fitted with Equation 2. Inset shows complete competition data for the NADH ligand; photobleaching or baseline drifting in this particular experiment probably caused the ~80% saturation.

(Figure 1A), while the N and C termini are located on the outside of the ring. This general arrangement is similar to that observed in MthK, where the Ca^{2+} ligands also flank the dimer interface (Figure 1D) facing the hole of the ring (Figure 1B) while the C-terminal "peripheral" subdomains lie outside the ring.

We determined the solution molecular weight of the RCK domain by size-exclusion chromatography coupled to light scattering (Folta-Stogniew and Williams, 1999). Measurements were performed at four protein concentrations in the range of 0.009 mg/ml to 1 mg/ml (0.55 μM to 61 μM). At all concentrations, the protein forms a single species with a solution molecular weight that varies between 133.4 and 135.9 kDa (Figure 1E). Since the expected monomer molecular weight is 16.3 kDa, the ratio between measured and expected masses gives an oligomer number of 8.2–8.3 molecules. These results, together with the crystal structure, clearly show that the KtrAB RCK domain adopts an octameric organization.

Ligand Binding

Simulated annealing omit maps were used to confirm the conformation of the bound NADH molecule (Figure 2A). The electron density shows that the adenine ring is flipped relative to the previously reported conformation (Roosild et al., 2002). The temperature factors of the adenine ring (average = 45.2 Å^2) are similar to those of the nearby main-chain atoms of the binding pocket (average = 41.6 Å^2), indicating that ligand is present at essentially 100% occupancy and that it is tightly held on the adenine end. Conversely, the ligand density in the omit map terminates before the second phosphate, revealing the nicotinamide end to be highly mobile.

The electron density of the partially resolved NADH ligand closely matches an ADP molecule, raising the question of whether ADP or ATP could also bind to this protein. To test this hypothesis, we determined whether the ATP fluorescent analog ATP-γS-BODIPY binds to the RCK domain. As shown in Figure 2B, when protein is added to a solution containing the analog, a decrease of BODIPY fluorescence intensity is observed along with a 3 nm spectral shift. The spectral changes reflect specifically the binding of the fluorescent analog to RCK since the addition of an excess of NADH reverses these effects due to competition for the same binding site (data not shown). Importantly, the fluorescence signal is also recovered

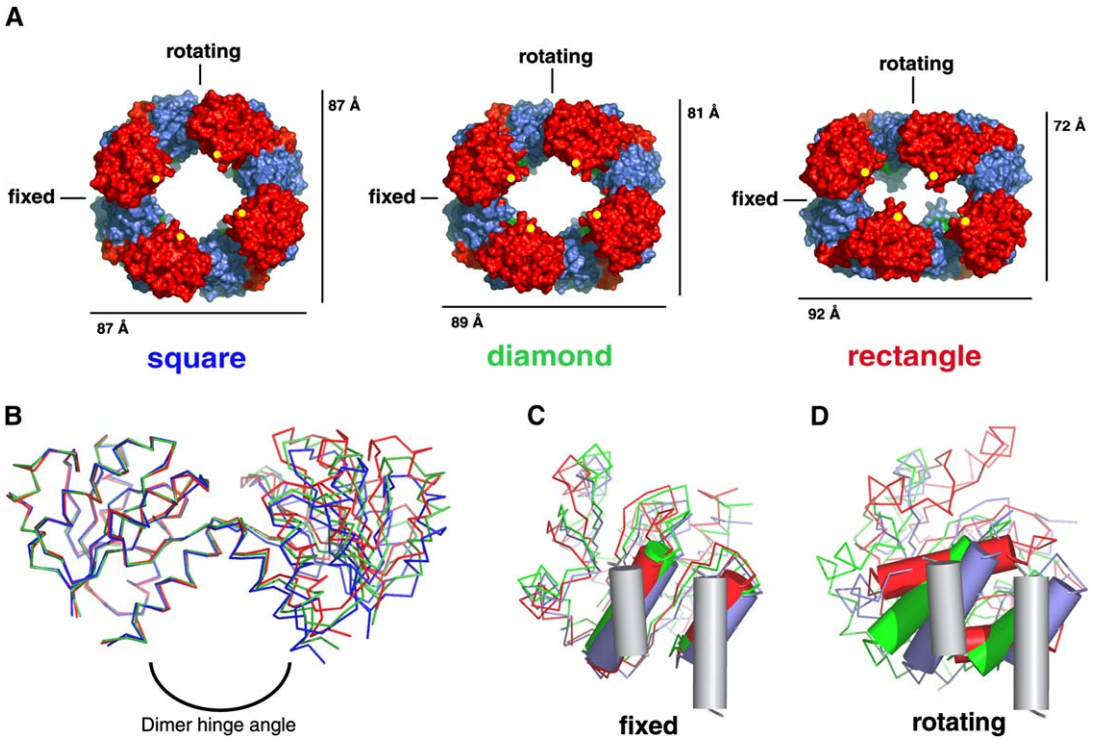

Figure 3. Three Ring Conformations

(A) Surface representations of the three ring conformations of the KtrAB RCK domain. Subunits are shown alternately in red and blue. Ligands are shown in green. Yellow spots mark the position of Asn38. External dimensions of the rings are indicated.

(B) Cα traces of homodimer assemblies from the square (blue), diamond (green), and rectangle (red) ring conformations superimposed through one of the subunits.

(C) View into the dimer-to-dimer fixed interface regions of the superimposed rings. Gray cylinders represent helices αD and αE from the superimposed subunit above the plane of the page (not shown). The other molecule is shown as a Cα trace with the two helices involved in the interaction (αD and αE) as cylinders; square, diamond, and rectangle conformations are shown in blue, green, and red, respectively. The longer cylinders on both sides of the interface correspond to the αD helix. Angle measurements discussed in the text correspond to relative rotation angle between αD helices in the two molecules.

(D) Same as (C) for the rotating interface.

upon competition with NAD^+, ATP (Figure 2B), ADP, and ATP-γS, but not with GTP-γS. An apparent dissociation constant (K_D) of ~600 nM was determined for ATP-γS-BODIPY (inset of Figure 2B), and competition experiments (Figure 2C) revealed that ATP-γS, ATP, and ADP bind more tightly ($K_D \sim$ 20–70 nM) to the domain than NADH or NAD^+ ($K_D \sim$ 200–400 nM). These results raise the possibility that, in the context of the KtrAB complex, this RCK domain may bind ATP or ADP. We cannot evaluate whether any of these small molecules are functionally active in KtrAB since no suitable ligand-dependent transport assay has been reported in the literature.

Cocrystallization trials under the same conditions were carried out using a variety of adenine-containing molecules (see Table S1 in the Supplemental Data available with this article online). All cocrystals show the same octameric ring structure, and only small adjustments in the ligand binding sites are observed. Just as for NADH, the NAD^+ maps also display a lack of electron density for the nicotinamide group. In all cases, the ligands are near full occupancy in all subunits as deduced by comparing the temperature factors of the adenine ring with the main-chain atoms of the binding pocket. This binding site uniformity demonstrates that the symmetry in our ring is not a result of the ligand's occupying only some of the sites in KtrAB but must be an intrinsic property of the octamer. Interestingly, we also observe for all cases that temperature factors of the ligand atoms increase when traveling away from the adenine group, indicating increased mobility (Figure 2A; see also Figure S1A). By contrast, the main-chain atoms of the binding pocket in that region do not show a similar pattern.

Other Conformations

Further crystallization trials of the KtrAB RCK domain were carried out, and determination of the structures (Table S1) revealed an octameric ring that adopts three different conformations, designated as square, diamond (discussed above), and rectangle (Figure 3A). The square conformation was determined at 3.0 Å in the presence of ATP

(R_{work} 26.4%, R_{free} 30.3%; PDB ID code 2HMW) or NADH (the two structures are basically identical); the diamond conformation was determined in the presence of NADH (2.2 Å, R_{work} 23.2%, R_{free} 25.8%; PDB ID code 2HMT), ATP-γS (2.25 Å, R_{work} 22.8% R_{free} 24.5%; PDB ID code 2HMU), ADP (2.2 Å, R_{work} 22.8%, R_{free} 24.5%; PDB ID code 2HMV), and NAD^+; and the rectangle conformation was determined in the presence of NADH (2.7 Å, R_{work} 21.4%, R_{free} 24.9%; PDB ID code 2HMS). Some of the diffraction data sets were collected after cryocooling the crystals using the high-pressure helium gas method (Kim et al., 2005). This method overcame difficulties encountered during the search for adequate cryoprotection conditions and ensured that the ligand was not disturbed by addition of cryoprotectants and remained at full occupancy. High-pressure cryocooling data sets were as good as or better than those obtained via traditional cryoprotection; no significant change was observed between ring structures determined with data obtained via these two methods.

The three ring structures differ in a few aspects. The overall shape and dimensions of the rings are different (Figure 3A). The outer ring diameter is 87 Å for the square, 89 Å and 81 Å for the diamond, and 92 Å and 72 Å for the rectangle (measured along the directions defined by the fixed and rotating interfaces, respectively); for MthK, this distance is 81 Å (see Figure S4). Therefore, the transition from square to rectangle results in a reduction of 15 Å in one direction (~7.5 Å for each half of the ring) and a smaller, concurrent 5 Å expansion in the other direction (~2.5 Å for each half of the ring). Strikingly, the square octamer ring is approximately 4-fold symmetrical, while the diamond and rectangle conformations exhibit 2-fold symmetry. The changes at the level of the inner hole of the ring can be illustrated by the separation of Asn38 Cα (marked as a yellow spot in Figure 3A) between pairs of domains positioned across the hole (opposing domains). This distance is 39 Å in the square conformation; in the diamond, it is 34 Å in one pair and 42 Å in the other; and in the rectangular ring, spacing is 22 Å in one pair versus 48 Å in the other. For comparison, the MthK ring is 4-fold symmetrical, with an inner diameter of 25 Å as measured from Asn145 Cα (the residue equivalent to Asn38).

Superimposition of individual subunits from the various rings shows almost no change (Figure 3B) except for a shift in the tip of the crossover helix. Between rings, the relative orientation of the two domains in a dimer changes by rotation about a hinge point close to Pro124 at the beginning of the crossover helix, with all motions occurring roughly in the same plane. This change can be measured in terms of the "dimer hinge angle" that corresponds to the relative angle between the crossover helices. Importantly, all four dimers within a given octameric ring have the same dimer hinge angle. The angles for each ring shape are ~80° in the square (blue), ~83.5° in the diamond (green), and ~90° in the rectangle (red). The 10° transition from square to rectangular ring causes a maximum displacement of 11 Å in the partner subunit. This results in a contraction on the face of the dimer that lines the hole of the ring. By contrast, the dimer hinge angle of MthK RCK is much larger, ~124°. In KtrAB, the total buried surface values for this interface change relatively little between conformations: 3277 $Å^2$ for the square, 3189 $Å^2$ for the diamond, and 3228 $Å^2$ for the rectangle.

The other regions that underlie the different ring shapes are the hydrophobic dimer-to-dimer interfaces. In the square conformation, all of the dimer-to-dimer interfaces are equivalent; in the rectangle and diamond rings, there are two different sets, rotating and fixed. Both sets utilize the same hydrophobic patch along helices αD and αE (Figure 1C and Figures 3C and 3D). The orientation of domains across the fixed interfaces (positioned along the long dimension in the diamond and rectangle conformations) remains almost unchanged in all three ring shapes (Figure 3C): The pair of helices (gray) in one domain pack against the equivalent pair from the other domain (blue, green, or red) with a relative angle of ~35°, ~38°, and ~37° and a total buried surface area of 1317 $Å^2$, 1628 $Å^2$, and 1544 $Å^2$ for the square, diamond, and rectangle, respectively. By contrast, in the rotating interfaces (along the short dimension of the diamond and rectangle rings), large relative domain movements occur (Figure 3D) (see Movie S1). In the diamond and rectangular conformations, the pairs of helices have rotated on each other and adopted a relative angle of ~46° (1167 $Å^2$ buried surface) and ~80° (1192 $Å^2$ buried surface), respectively, while in the square conformation, this interface is identical to the fixed interface (~35°). The orientation of domains across this interface when viewed relative to those seen in the square corresponds to a 45° rotation for the rectangle and an 11° rotation for the diamond (with half of the rotation coming from each domain). By comparison, in MthK, the corresponding angle between pairs of helices forming the dimer-to-dimer interfaces is ~82°. Interestingly, the total surface area buried on protein-protein contacts within each ring remains almost constant (about 18,370 $Å^2$) in all three shapes.

Global Movements

The three ring conformations form a continuum of structural changes between the two extremes, square and rectangle, and to dissect the overall movements between conformations, we will only consider these two ring shapes. Half-rings consisting of two homodimers from each conformation were superimposed through the domains flanking the fixed interface (Figure 4A). The tips of this C-shaped unit flex when the homodimer assembly hinge angle closes or opens. These regions of greatest movement in the halves of the ring come into contact with their counterparts across the rotating interface. As described above, the flexing of the "C" is accommodated by a relatively small outward translation along the fixed interface (Figure 3A). Superposition of the complete rings reveals that this change is also accompanied by a rigid-body rotation

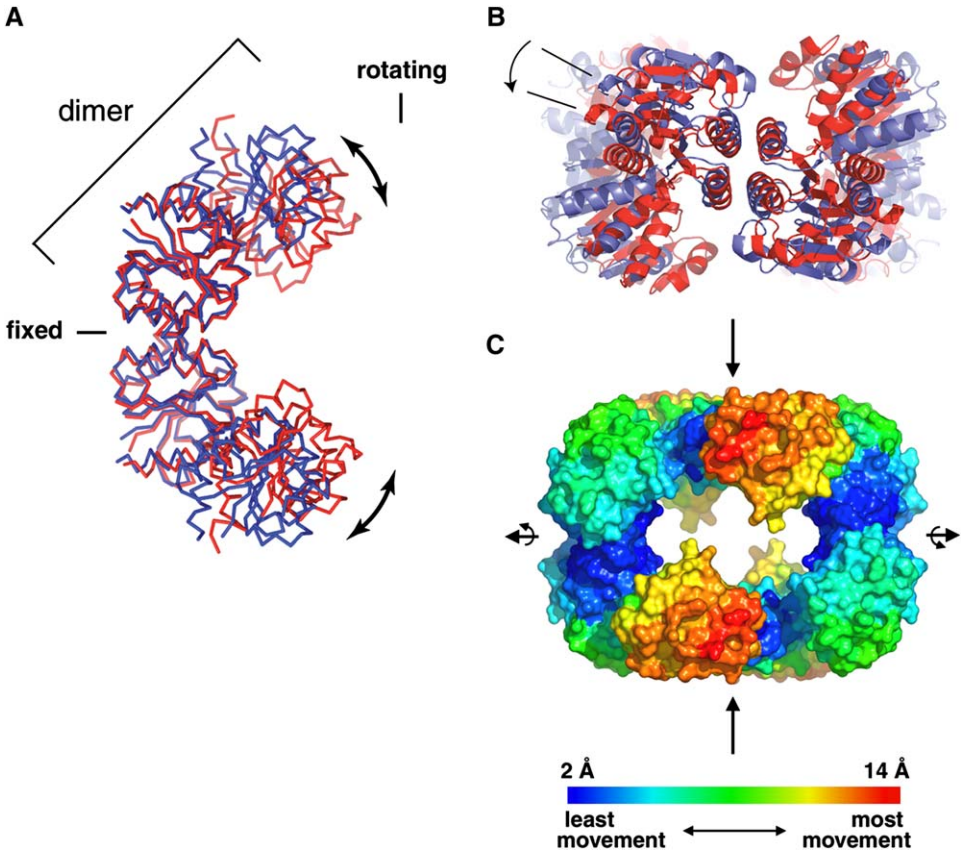

Figure 4. Conformational Changes

(A) Half-rings of the square (blue) and rectangle (red) conformation structures were generated by breaking the octamers at the rotating interfaces. The Cα traces of the resulting tetramers were superimposed through their fixed interfaces. Arrows mark conformational shifts resulting from changes in the dimer hinge angle.

(B) Superimposed square (blue) and rectangle (red) rings as viewed down the fixed-interface dyad axis. Lines mark the position of the same helix in the two conformations. An arrow between marked helices demonstrates the half-ring rigid-body rotation around the fixed-interface dyad.

(C) Surface representation of the rectangle ring structure. Each residue is colored according to the Cα atom magnitude of displacement between the square and rectangle conformations. The colored-coded bar represents a range of displacements between 2 and 14 Å. Regions in red and orange exhibit the greatest movement. Arrows indicate the direction and relative magnitude of overall square-to-rectangle conformational changes; slight rotation about the fixed interface axis shown in (B) is also indicated.

of the whole half-ring about the fixed interface dyad axis (Figure 4B), with the two halves of the ring rotating in opposite directions.

The motions occurring in the KtrAB RCK ring can be viewed by measuring the movement of each Cα atom in the transition from the most open form (square) to the most closed (rectangle) and plotting the distance values onto the rectangular ring using a rainbow color-coded representation as shown in Figure 4C (see also Movie S1). Regions of greatest movement are colored red, and those of least movement are blue. The movements in the down-domains mirror the movements in the up-domains. This representation shows that the greatest movement of the ring occurs mainly along one dimension, on the domains flanking the rotating interface. This shows that two of the four domains on the top face of the ring move significantly more during ring transitions.

The KtrAB Complex

To gain an understanding of the interactions between the RCK-domain ring and the associated KtrB membrane protein, we conducted a series of biochemical experiments both with the KtrB membrane protein alone and with the KtrAB complex. Membrane preparations of cells expressing KtrB were exposed to a bifunctional amino-group crosslinker, DSP. Western blot analysis (Figure 5A) revealed a band shift from around 41 kDa to approximately 83 kDa. The expected molecular weight of the polypeptide is 49 kDa, and these results suggest that KtrB is a dimer in the membrane. Size-exclusion chromatography coupled to light scattering, UV absorbance, and refractive index measurements (SEC-LS/UV/RI) of purified detergent-solubilized KtrB protein (Figure 5B) showed that the solution molecular weight of the protein is 98 kDa. The protein associates with detergent and lipid molecules to form

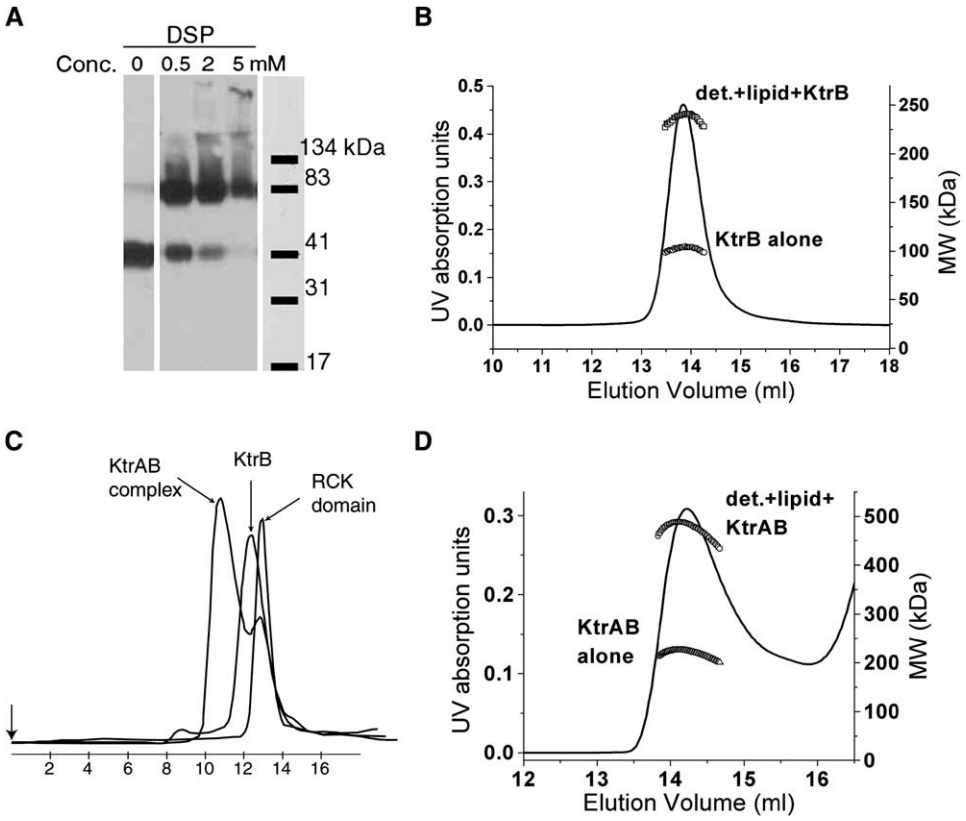

Figure 5. KtrB and the Complex

(A) Western blot of membrane preparations containing His-tagged KtrB protein. Membrane preparations were mixed with increasing concentrations of DSP, a bifunctional amino-group crosslinker. The blot was probed with anti-His-tag monoclonal antibody.

(B) Light-scattering measurements of the KtrB membrane protein in the presence of detergent (dodecyl maltoside). The continuous line corresponds to the UV elution profile from a Superdex 200 column. The points above the UV trace are the determined solution molecular weight of the macromolecule plus or minus associated detergent/lipid at different points of the eluted protein peak.

(C) Superimposed UV elution profiles from a Superdex 200 size-exclusion column of KtrB, the RCK domain alone, and of a mixture of the two proteins. Arrow on the left indicates injection time.

(D) Light-scattering experiments with the KtrAB complex. Details as in (B), but the experiment was performed in a Superose 6 size-exclusion column. The peak emerging after 16 ml elution volume is RCK domain, as there was excess of this protein in the injected mixture. The elution volumes of the different experiments depicted in (B)–(D) cannot be compared directly.

a complex with a total molecular weight of 238 kDa. This technique has been successfully applied to the determination of the oligomer number of several membrane proteins: maltoporin, α-hemolysin, bacterial glutamate transporter (Yernool et al., 2003), and the MlotiK1 potassium channel (Clayton et al., 2004). Together, these results strongly indicate that the KtrB membrane protein exists as a stable dimer both in the membrane and in solution.

Size-exclusion chromatography elution profiles of mixtures of purified KtrB membrane protein and truncated RCK domain show a different species that elutes ahead of its individual components (Figure 5C). SDS-PAGE of fractions from the new peak revealed the presence of both the KtrB and RCK-domain proteins (data not shown). We estimated that two to four KtrB protein molecules bind to eight RCK domains by performing titration experiments in which the molar ratios of KtrB and RCK domain were altered and size-exclusion elution profiles were monitored for the formation of the complex peak and disappearance of either of the individual components (data not shown). The KtrAB protein complex was analyzed by SEC-LS/UV/RI (Figure 5D). Since protein concentration is a factor in the determination of the molecular weight, several stoichiometry models and associated theoretical extinction coefficients were considered. A model with stoichiometry of eight RCK domains plus two KtrB proteins (total expected molecular weight of 228 kDa) resulted in the best match with the calculated molecular weight (a difference of −1 kDa). In contrast, a model with eight RCK domains plus four KtrB proteins resulted in a discrepancy of −75 kDa between the expected and calculated values, while a model with eight RCK domains plus one KtrB protein had a discrepancy of +30 kDa.

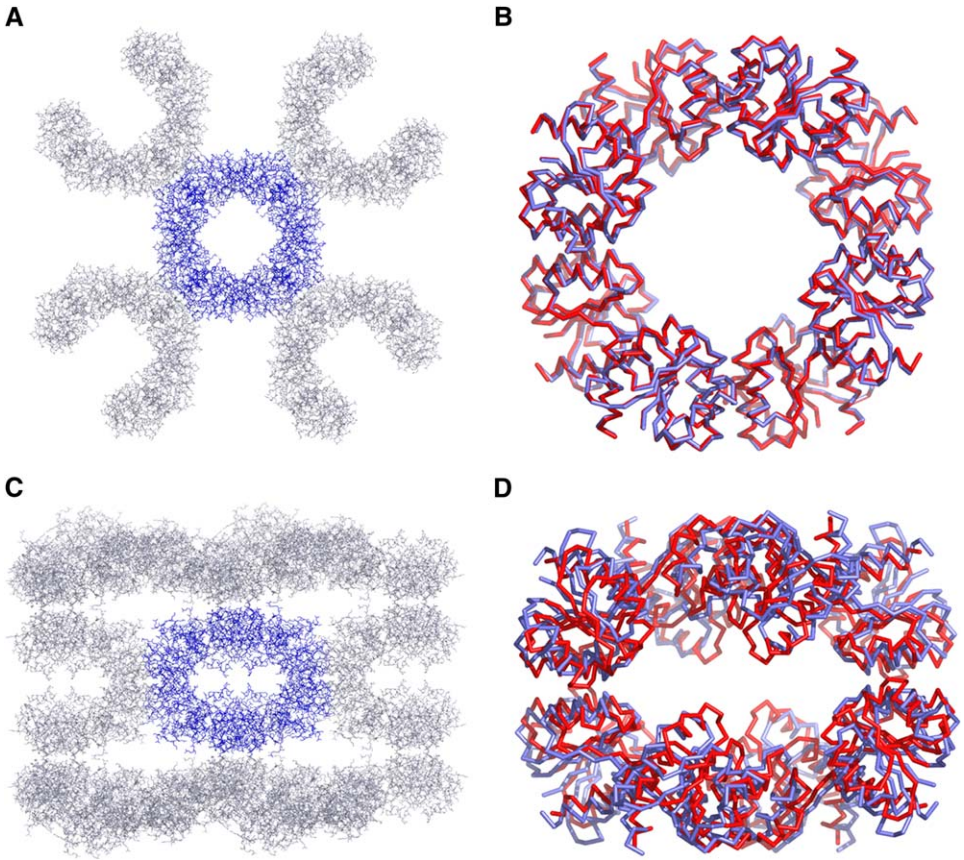

Figure 6. Other RCK-Domain Structures

(A) Stick representation of molecules forming the crystal lattice of previously reported coordinates (PDB ID code 1LSU) (KtrAB RCK domain). An octameric ring is shown at the center in blue.

(B) Superimposition of our square ring (blue) and the octameric ring present in the crystal lattice of the 1LSU coordinates (red).

(C) Stick representation of molecules forming the crystal lattice of previously reported coordinates (PDB ID code 1LSS) (Trk RCK domain). An octameric ring is shown at the center in blue.

(D) Superimposition of our rectangle ring (blue) and the octameric ring present in the crystal lattice of the 1LSS coordinates (red).

DISCUSSION

This study has shown that the RCK domains of the KtrAB transporter and MthK channel share the same fold, have partially overlapping ligand sites, and form octameric rings with similar up-and-down architecture.

How then do we resolve our findings with the previous crystal structures of the KtrAB RCK domain (PDB ID code 1LSU) and of the Trk RCK domain (PDB ID code 1LSS), which form the basis of the tetrameric model (Roosild et al., 2002)? To address this issue, we analyzed the crystal lattices of the coordinates available from the Protein Data Bank and discovered that both of these proteins, in fact, also form octameric rings (Figures 6A and 6C). The protein construct used in the 1LSU crystal structure is the same one that we have used in our experiments, and the structure is indistinguishable from the square conformation presented above (Figure 6B). The 1LSS structure (this is a different RCK-domain protein) forms a ring (Figure 6D) that is very similar to our rectangular conformation but is even slightly more closed. Our light-scattering experiments (see Supplemental Data) performed with the Trk RCK domain revealed a 132 kDa octamer in solution (expected molecular weight of monomer is 16.5 kDa). Altogether, these results strongly support the notion that the biologically active form of the RCK family is an octamer ring.

RCK domains are thought to regulate ion transport by undergoing a conformational change induced by binding ligand (Jiang et al., 2002a). However, we have determined different conformations of the KtrAB RCK ring with the same bound ligand (for example, NADH is present in octamers adopting all three conformations, while ATP is found in structures adopting both the square and diamond conformations). We propose that the energetics of the ring have been altered in the absence of KtrB and that our structures are sampling conformational states that are now independent of the nature of the bound ligand. This proposal also provides an explanation for the dissociation constants of the ligands (20–400 nM), values that are

intriguingly tight for a physiological regulatory role (for example, in *E. coli*, the intracellular concentrations of ATP and ADP are in the low mM and hundreds of μM range, respectively [Canonaco et al., 2003; Jensen et al., 1999]).

A salient difference between the RCK-domain octamers of the MthK channel and the KtrAB ion transporter is the symmetry of the rings. In the MthK channel, both the RCK ring and the membrane protein part (which has four identical subunits adopting the TM-P loop-TM repeat architecture) are 4-fold symmetrical in the active (open) and inactive (closed) states (Doyle et al., 1998; Jiang et al., 2002b; Ye et al., 2006 [this issue of *Cell*]). In contrast, the KtrAB RCK ring can be either 2-fold or 4-fold symmetrical (Figure 3A), while the KtrB membrane protein is an asymmetrical molecule; a single KtrB polypeptide is expected to have four nonidentical TM-P loop-TM repeats (Durell et al., 1999; Nakamura et al., 1998; Tholema et al., 1999) connected by very different cytoplasmic loops. We have now shown (Figures 5A and 5B) that the KtrB protein forms a dimer both in the membrane and in solution (in presence of detergent). Moreover, we also show (Figures 5C and 5D) that the stoichiometry of the complex between the RCK domain and the KtrB membrane protein (the KtrAB complex) is eight RCK domains to two KtrB proteins, corresponding in all likelihood to one RCK octamer ring associated with a KtrB dimer. A simple explanation for the observed ring shapes results from the good assumption that the KtrB membrane-protein dimer is 2-fold symmetrical (Goodsell and Olson, 2000) and, therefore, that in the KtrAB complex, the symmetries of the membrane-protein part and RCK ring are matched (note that a 4-fold symmetry operation contains within it a 2-fold symmetry relation).

The dimeric KtrB was modeled by placing two potassium ion-channel pores side by side related by a 2-fold axis; this provides an approximated KtrB dimer pore-to-pore distance of ~50 Å. To match the KtrB dimer to the RCK-domain octamer, we have looked for two opposing binding sites on the ring that satisfy two criteria: (1) proper spacing and (2) an unobstructed ion pathway. We found two sets of sites that fit these criteria in the deep grooves formed by the up-and-down stacking of the RCK subunits (Figures 7A and 7B). The centers of these regions are separated by about 60 Å, which is more than sufficient to fit the KtrB dimer model (Figures 7C and 7D), and the depth of the grooves allows easy access between bulk solution and the ion-transport pathway. The relation between the two KtrB molecules in the membrane-protein dimer model was not altered to fit the different ring shapes. Interestingly, a second-site suppressor experiment in the *E. coli* KefC protein (Roosild et al., 2002), which has a C-terminally tethered RCK domain, suggests a direct contact between a cytoplasmic loop of the membrane-protein part and the crossover helix of the RCK domain. This contact position correlates to Gln134 in the RCK of KtrAB and maps into the grooves of our ring structures (Figure 7B), suggesting by analogy that a KtrB cytoplasmic loop (14 to 35 residues in length) may also bind in the same region.

The two sets of potential binding sites differ in an important way: One set experiences major structural changes during the transition from the square to the rectangle conformation, while the other set does not. For example, in the unchanging sites, the distances separating the two sides of the groove (between Glu40 Cα and Asn61 Cα) are 25.8 Å in the square and 27.7 Å in the rectangle. By contrast, in the changing sites, the equivalent distances are 25.8 Å (square) and 14.6 Å (rectangle) (Figures 7A and 7B). The reason for the large change is that the very mobile face of an up-domain forms one of the sides of this groove (Figure 4C and Movie S2). We favor the set of changing sites as the binding region for the KtrB molecules since these seem to provide the most obvious way of transmitting the conformational change from the RCK ring to the membrane protein. This model not only provides an easy fit between the membrane-protein dimer and the RCK ring but also readily accommodates the specific conformation mechanics observed for the ring (square, diamond, and rectangle) without an obvious need for large changes in the relative position of the monomers within the KtrB dimer.

The structural parallels between the MthK potassium channel and the KtrAB ion transporter (the octamer ring of the RCK domain plus the four TM-P loop-TM repeat membrane-protein architecture) probably mean that, like in channels, activation of ion transport in KtrAB occurs by a conformational change in the cytoplasmic regions of the membrane protein induced by a structural movement in the RCK octameric ring. This equivalence provides us with clues about the functional meaning of the three ring conformations (Figure 3A). A comparison (Jiang et al., 2002a, 2002b; Ye et al., 2006) of the MthK RCK octamer with and without calcium ions shows that channel activation correlates with a decrease of the dimer hinge angle in the homodimer assemblies and a resulting expansion of the ring. In the KtrAB transporter, the transition from the rectangle to the square rings (Figure 3B) follows a similar trend: Decrease in the hinge angle is correlated with a major expansion of the ring in one direction and a much smaller contraction in the other. Interestingly, in our models of the KtrAB complex (Figures 7C and 7D), the global conformational changes are reflected as a local expansion of the ring regions in close proximity to the cytoplasmic mouth of each membrane protein. Altogether, these observations evoke an equivalent functional transition from inactive to active.

In conclusion, we envisage that, during activation of KtrAB ion transport, an adenine-containing ligand binds to an inactive (rectangular-like) RCK-ring conformation. Ligand binding alters the relative orientation of the two domains of the homodimer assembly, resulting in a closing of the dimer hinge angle. The net effect is that the ring expands along the direction defined by the rotating interfaces and contracts a smaller amount along the perpendicular direction; the ring adopts a square-like shape. These conformational changes are propagated to the membrane-protein dimer by matching movements of one

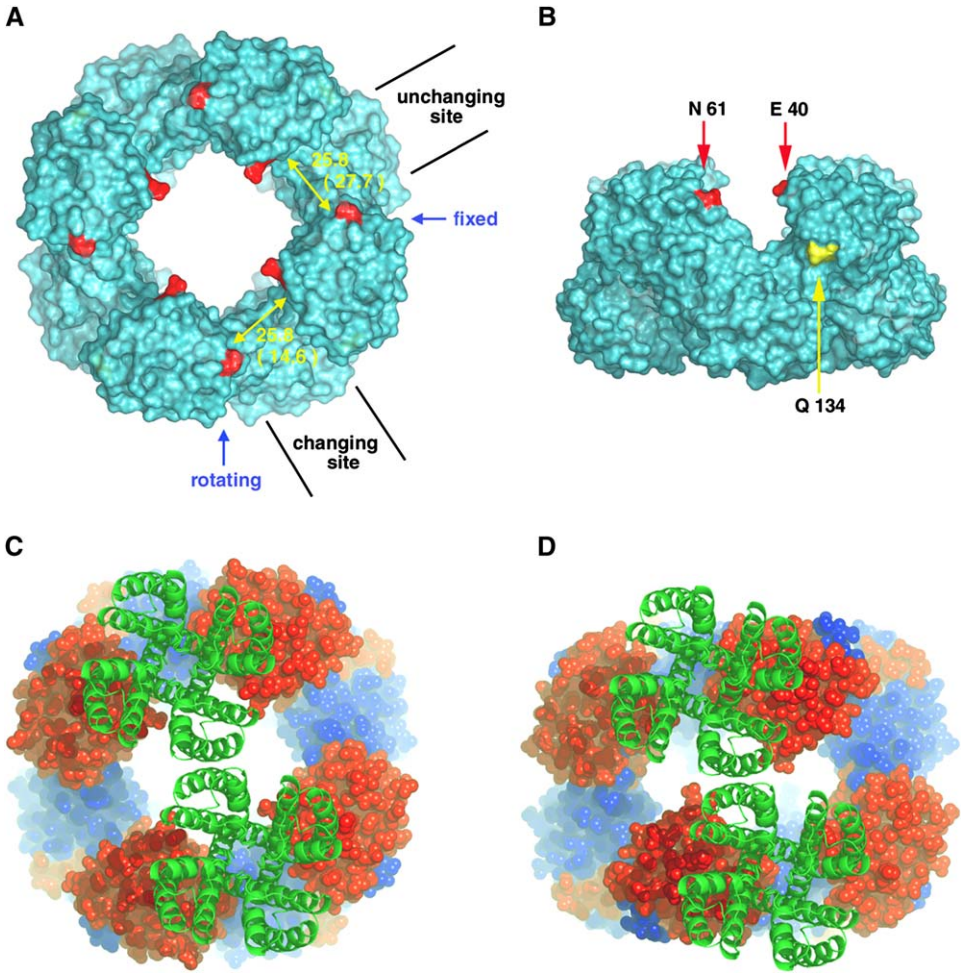

Figure 7. Modeling Interactions between KtrB and RCK Domain

(A) Top view of the square ring, with positions of Glu40 and Asn61 marked (red). Arrows indicate the relative positions of the Cα atoms of these residues. The distances (in Å) separating the two atoms are shown for the square and rectangle (in parenthesis) conformations.

(B) Side view of square ring, looking into one of the deep grooves, with residues 40 and 61 in red and Gln134 marked in yellow.

(C) Top view of proposed KtrAB model with the square ring. The KtrB dimer is approximated by two side-by-side KcsA potassium-channel molecules shown in green ribbon. The KtrAB RCK square ring is shown in the background as a CPK representation with alternate subunits in red and blue.

(D) Top view of the proposed KtrAB model with the rectangle ring. As in (C), but with the RCK rectangular ring. Details of the actual gating motions within the membrane protein remain unknown, and we have not attempted to depict them here.

or more of the cytoplasmic loops that bind to the ring, resulting in ion transport.

EXPERIMENTAL PROCEDURES

Protein Expression and Purification

A truncated form (Roosild et al., 2002) (residues 1–144 and mutation C22V) of the *KtrA* gene of *Bacillus subtilis* was subcloned into a pet15b vector (Novagen). Before induction, the culture was cold-shocked by transferring to a water/ice bath for 30 min followed by the addition of 2%–3% (v/v) ethanol; growth was allowed to continue at 20°C for 10 hr. The cell pellet was resuspended in lysis buffer (120 mM NaCl, 30 mM KCl, 50 mM Tris [pH 8.5]) with protease inhibitors. Protein was purified in a cobalt-agarose column (BD Biosciences). Eluted protein (with thrombin added to cleave the His tag) was dialyzed overnight at 4°C against lysis buffer plus 1 mM DTT. Protein was further purified in a Superdex 200 size-exclusion chromatography column equilibrated with lysis buffer, spin-concentrated to 6 mg/ml, and dialyzed against the final buffer (30 mM NaCl, 7 mM KCl, 12 mM Tris [pH 8.5], 1 mM DTT). The truncated RCK domain of the Trk ion transporter from *M. jannaschii* was cloned into pet24d and purified as described (Roosild et al., 2002) with minor modifications.

The KtrB protein from *Bacillus subtilis* was cloned into a pet15b vector and expressed in *E. coli* at 37°C. KtrB was extracted from the membrane by incubation with the detergent dodecyl maltoside (40 mM). The preparation was centrifuged at 34,500 × g for 45 min. The supernatant was loaded into a cobalt-agarose column for affinity His-tag purification; the tag was removed by overnight incubation with thrombin. Protein was concentrated and loaded into a size-exclusion chromatography column equilibrated with 50 mM Tris (pH 7.5), 120 mM NaCl, 30 mM KCl, 1 mM dodecyl maltoside, 5 mM DTT. Titration experiments with the KtrAB complex were performed in the same buffer.

Crosslinking Experiments

Membranes of *E. coli* cells expressing KtrB protein were prepared by cell lysis, followed by 10 min spin at 10,000 rpm (Sorvall rotor SS34) and a high-speed spin at 50,000 rpm (Beckman rotor Ti-70) for 1.5 hr at 4°C. Pellets were resuspended in 1 ml of 0.1 M sodium phosphate (pH 7.5). Total protein concentration was determined by a colorimetric assay (Bio-Rad). The suspension was diluted to 5–10 mg/ml protein, and crosslinker DSP (dithiobis(succinimidyl propionate)), at 50 mM in DMSO, was added to 25 μl membrane aliquots and incubated at room temperature for 30 min. Reactions were stopped by addition of Tris buffer solution (pH 7.5) to a final concentration of 50 mM and incubated for 15 min. Samples were analyzed by western blot probed with an anti-His-tag monoclonal antibody (QIAGEN).

Crystallization

Cocrystallization trials of the KtrAB RCK domain were carried out using a variety of ligands, including NADH, NAD, ATP, ATP-γS, ADP, cAMP, and GTP-γS. Fresh ligand (1 mM to 2 mM) was typically added to the protein solution just prior to setting up the drops. Extensive screening of potential crystallization conditions using the sitting-drop method yielded three crystal forms at 20°C. The I422 crystals (square ring) and P422 crystals (diamond ring) were grown over a well solution containing 500 mM $MgCl_2$, 50 mM Tris (pH 8.8), and 8.5% PEG 2000. The $P3_112$ crystals (rectangular ring) were grown in the presence of KtrB over a well of 100 mM sodium acetate (pH 5.2) and 2 M sodium formate. These crystals were grown under a thin layer of paraffin oil.

Crystal Cryocooling

The $P3_112$ crystals were frozen directly in the nitrogen stream. The I422 and P422 crystals were cryoprotected by passing through a series of modified well solutions with increasing amounts of cryoprotectants (glycerol or ethylene glycol) and ~2 mM of the appropriate ligand. Crystals were then either frozen directly in the nitrogen stream or flash frozen in liquid nitrogen. Despite the high quality of the data collected from crystals prepared with this approach, the ligand density in resulting maps varied markedly. High-pressure cooling (Kim et al., 2005) was subsequently employed on some of the crystals to achieve freezing without adding cryoprotectant and disturbing the ligand.

Data Collection/Processing and Structure Determination

Data were collected at beamline X25 of the NSLS or beamlines A1 and F1 of the Cornell High Energy Synchrotron Source (CHESS) and processed using HKL2000 (Otwinowski and Minor, 1997). Molecular replacement was carried out with MOLREP using a single domain of the RCK protein (PDB ID code 1LSU) as a search model. Refinement was carried out using CNS (Brunger et al., 1998) with iterative rounds of model building in O (Jones et al., 1991). Coordinate manipulations and superimpositions were performed using the CCP4 package of programs (http://www.ccp4.ac.uk/main.html).

Light-Scattering Studies

KtrAB RCK domain samples at four different dilutions (0.009, 0.1, 0.5, and 1 mg/ml) were injected into a Superdex 200 size-exclusion column equilibrated with 20 mM HEPES (pH 8.0), 150 mM KCl, 1 mM EDTA. A Trk RCK domain sample at 1 mg/ml was injected into a Superdex 200 size-exclusion column equilibrated with 50 mM Tris (pH 8.5), 120 mM NaCl, 30 mM KCl, 1 mM DTT. Light scattering, UV absorbance, and refractive index measurements were done on the eluted peak. Weight-average molar mass was determined by solving the equation that relates the mass of the solute to its concentration and the excess scattered light, measured at several angles (Folta-Stogniew and Williams, 1999).

KtrB alone or a mixture of KtrB and RCK domain in 50 mM Tris (pH 8.5), 120 mM NaCl, 30 mM KCl, 5 mM DTT, 1 mM dodecyl maltoside at a concentration of 1–2 mg/ml was injected into a Sephadex 200 or Superose 6 size-exclusion column. Light scattering, UV absorbance, and refractive index measurements were performed on the eluted peaks. The protein molecular weight was determined by combinations of these measurements as described in the literature (Arakawa et al., 1992; Folta-Stogniew, 2006; Folta-Stogniew and Williams, 1999; Hayashi et al., 1989; Yernool et al., 2003). The total protein-detergent complex molecular weight was determined from Debye plots of light scattered versus scattering angle.

Fluorescence Experiments

Fluorescence measurements were carried out at 25°C in 50 mM Tris-HCl (pH 7.5), 150 mM NaCl. Excitation and emission wavelengths were 490 and 506 nm, respectively. Data were fitted with SigmaPlot software (Jandel). Binding of the fluorescent ATP analog ATP-γS-BODIPY to the KtrAB RCK domain was determined from the decrease in BODIPY fluorescence intensity after addition of aliquots of concentrated stock solution of protein to 10 nM of ATP-γS-BODIPY. The experimental data were fit to Equation 1,

$$I = \frac{I_{max} K_D}{K_D + [protein]} + I_0, \quad (1)$$

where [protein] represents different concentrations of protein (the total concentration of protein in the cuvette from the experimental conditions is practically equivalent to the free concentration of the protein) and I is the fluorescence emission at different values of [protein]. I_{max} and I_0 are the emission values in the absence of protein and at infinite protein concentration, respectively. K_D is the dissociation constant. Protein concentration and fluorescence intensity were corrected for sample dilution.

Binding affinities of the ligands to protein were measured by competitive binding experiments with ATP-γS-BODIPY. ATP-γS-BODIPY and protein were mixed at concentrations of 0.3 μM and 1.4 μM, respectively. The fluorescence emission of ATP-γS-BODIPY was recorded for each addition of ligand from concentrated stocks. The relative change of ATP-γS-BODIPY fluorescence, ΔF, expressed as a percentage was calculated as

$$\Delta F = \frac{(F - F_{min})}{(F_{max} - F_{min})} \times 100,$$

where F_{min} and F_{max} are the fluorescence intensity in the absence and presence of a saturating concentration of ligand, respectively. F is the fluorescence intensity at each ligand concentration. To ensure that 100% of ATP-γS-BODIPY was displaced from the binding site, 50 μM ATP was added at the end of the titration to verify that no change in fluorescence intensity was detected. The data from these titration experiments were fit to Equation 2:

$$\Delta F = \frac{\Delta F_{max}[L]}{[L] + K_{app}}. \quad (2)$$

$[L]$ is the ligand concentration, ΔF_{max} is the maximum relative change of fluorescence, and K_{app} is the apparent equilibrium dissociation constant. The equilibrium dissociation constant (K_D) for each ligand was corrected with

$$K_D = \frac{K_{app}}{1 + ([\mathrm{ATP} - \gamma S - BODIPY]/K_{D1})},$$

where [ATP-γS-BODIPY] is the concentration of the fluorescent ligand preincubated with the sample (0.3 μM) and K_{D1} is the equilibrium dissociation constant for ATP-γS-BODIPY determined above.

Supplemental Data

Supplemental Data include Supplemental References, four figures, one table, and two movies and can be found with this article online at http://www.cell.com/cgi/content/full/126/6/1147/DC1/.

ACKNOWLEDGMENTS

We thank the lab members, L. Heginbotham, Y. Modis, and E. De La Cruz for support and advice. We also thank Y. Jiang and the L. Regan

lab. Our special thanks to E. Folta-Stogniew at the Keck Facility, Yale University, for performing the SEC-LS/UV/RI. We also thank the staff at X25, NSLS, and CHESS. J.-L.V.I. is a fellow of the American Heart Association. Support for this work came in part from funds to J.H.M.-C. from the Hellman Family Foundation and the National Institutes of Health (GM 068585).

Received: February 18, 2006
Revised: May 22, 2006
Accepted: August 11, 2006
Published: September 21, 2006

REFERENCES

Arakawa, T., Langley, K.E., Kameyama, K., and Takagi, T. (1992). Molecular weights of glycosylated and nonglycosylated forms of recombinant human stem cell factor determined by low-angle laser light scattering. Anal. Biochem. *203*, 53–57.

Bellamacina, C.R. (1996). The nicotinamide dinucleotide binding motif: a comparison of nucleotide binding proteins. FASEB J. *10*, 1257–1269.

Brunger, A.T., Adams, P.D., Clore, G.M., DeLano, W.L., Gros, P., Grosse-Kunstleve, R.W., Jiang, J.S., Kuszewski, J., Nilges, M., Pannu, N.S., et al. (1998). Crystallography & NMR system: A new software suite for macromolecular structure determination. Acta Crystallogr. D Biol. Crystallogr. *54*, 905–921.

Canonaco, F., Schlattner, U., Wallimann, T., and Sauer, U. (2003). Functional expression of arginine kinase improves recovery from pH stress of Escherichia coli. Biotechnol. Lett. *25*, 1013–1017.

Clayton, G.M., Silverman, W.R., Heginbotham, L., and Morais-Cabral, J.H. (2004). Structural basis of ligand activation in a cyclic nucleotide regulated potassium channel. Cell *119*, 615–627.

Dong, J., Shi, N., Berke, I., Chen, L., and Jiang, Y. (2005). Structures of the MthK RCK domain and the effect of Ca2+ on gating ring stability. J. Biol. Chem. *280*, 41716–41724.

Doyle, D.A., Morais Cabral, J., Pfuetzner, R.A., Kuo, A., Gulbis, J.M., Cohen, S.L., Chait, B.T., and MacKinnon, R. (1998). The structure of the potassium channel: molecular basis of K+ conduction and selectivity. Science *280*, 69–77.

Durell, S.R., Hao, Y., Nakamura, T., Bakker, E.P., and Guy, H.R. (1999). Evolutionary relationship between K(+) channels and symporters. Biophys. J. *77*, 775–788.

Epstein, W. (2003). The roles and regulation of potassium in bacteria. Prog. Nucleic Acid Res. Mol. Biol. *75*, 293–320.

Folta-Stogniew, E. (2006). Oligomeric states of proteins determined by size-exclusion chromatography coupled with light scattering, absorbance and refractive index detectors. In Methods in Molecular Biology: New and Emerging Proteomics Techniques, D. Nedelkov and R. Nelson, eds. (Totowa, NJ, USA: Humana Press), pp. 97–112.

Folta-Stogniew, E., and Williams, K.M. (1999). Determination of molecular masses of proteins in solution:implementation of an HPLC size exclusion chromatography and laser light scattering service in a core laboratory. J. Biomol. Tech. *10*, 51–63.

Goodsell, D.S., and Olson, A.J. (2000). Structural symmetry and protein function. Annu. Rev. Biophys. Biomol. Struct. *29*, 105–153.

Hayashi, Y., Matsui, H., and Takagi, T. (1989). Membrane protein molecular weight determined by low-angle laser light-scattering photometry coupled with high-performance gel chromatography. Methods Enzymol. *172*, 514–528.

Jensen, P.R., Van Der Weijden, C.C., Jensen, L.B., Westerhoff, H.V., and Snoep, J.L. (1999). Extensive regulation compromises the extent to which DNA gyrase controls DNA supercoiling and growth rate of Escherichia coli. Eur. J. Biochem. *266*, 865–877.

Jiang, Y., Pico, A., Cadene, M., Chait, B.T., and MacKinnon, R. (2001). Structure of the RCK domain from the E. coli K+ channel and demonstration of its presence in the human BK channel. Neuron *29*, 593–601.

Jiang, Y., Lee, A., Chen, J., Cadene, M., Chait, B.T., and MacKinnon, R. (2002a). Crystal structure and mechanism of a calcium-gated potassium channel. Nature *417*, 515–522.

Jiang, Y., Lee, A., Chen, J., Cadene, M., Chait, B.T., and MacKinnon, R. (2002b). The open pore conformation of potassium channels. Nature *417*, 523–526.

Jones, T.A., Zou, J.Y., Cowan, S.W., and Kjeldgaard. (1991). Improved methods for building protein models in electron density maps and the location of errors in these models. Acta Crystallogr. A *47*, 110–119.

Kim, C.U., Kapfer, R., and Gruner, S.M. (2005). High-pressure cooling of protein crystals without cryoprotectants. Acta Crystallogr. D Biol. Crystallogr. *61*, 881–890.

Kuo, M.M., Haynes, W.J., Loukin, S.H., Kung, C., and Saimi, Y. (2005). Prokaryotic K(+) channels: from crystal structures to diversity. FEMS Microbiol. Rev. *29*, 961–985.

Loukin, S.H., Kuo, M.M., Zhou, X.L., Haynes, W.J., Kung, C., and Saimi, Y. (2005). Microbial K+ channels. J. Gen. Physiol. *125*, 521–527.

Matsuda, N., Kobayashi, H., Katoh, H., Ogawa, T., Futatsugi, L., Nakamura, T., Bakker, E.P., and Uozumi, N. (2004). Na+-dependent K+ uptake Ktr system from the cyanobacterium Synechocystis sp. PCC 6803 and its role in the early phases of cell adaptation to hyperosmotic shock. J. Biol. Chem. *279*, 54952–54962.

Munro, A.W., Ritchie, G.Y., Lamb, A.J., Douglas, R.M., and Booth, I.R. (1991). The cloning and DNA sequence of the gene for the glutathione-regulated potassium-efflux system KefC of Escherichia coli. Mol. Microbiol. *5*, 607–616.

Nakamura, T., Yuda, R., Unemoto, T., and Bakker, E.P. (1998). KtrAB, a new type of bacterial K(+)-uptake system from Vibrio alginolyticus. J. Bacteriol. *180*, 3491–3494.

Otwinowski, Z., and Minor, W. (1997). Processing of X-ray diffraction data collected in oscillation mode. Methods Enzymol. *276*, 307–326.

Roosild, T.P., Miller, S., Booth, I.R., and Choe, S. (2002). A mechanism of regulating transmembrane potassium flux through a ligand-mediated conformational switch. Cell *109*, 781–791.

Schlosser, A., Hamann, A., Bossemeyer, D., Schneider, E., and Bakker, E.P. (1993). NAD+ binding to the Escherichia coli K(+)-uptake protein TrkA and sequence similarity between TrkA and domains of a family of dehydrogenases suggest a role for NAD+ in bacterial transport. Mol. Microbiol. *9*, 533–543.

Tholema, N., Bakker, E.P., Suzuki, A., and Nakamura, T. (1999). Change to alanine of one out of four selectivity filter glycines in KtrB causes a two orders of magnitude decrease in the affinities for both K+ and Na+ of the Na+ dependent K+ uptake system KtrAB from Vibrio alginolyticus. FEBS Lett. *450*, 217–220.

Tholema, N., Vor der Bruggen, M., Maser, P., Nakamura, T., Schroeder, J.I., Kobayashi, H., Uozumi, N., and Bakker, E.P. (2005). All four putative selectivity filter glycine residues in KtrB are essential for high affinity and selective K+ uptake by the KtrAB system from Vibrio alginolyticus. J. Biol. Chem. *280*, 41146–41154.

Ye, S., Li, Y., Chen, L., and Jiang, Y. (2006). Crystal structures of a ligand-free MthK gating ring: insights into the ligand gating mechanism of K+ channels. Cell *126*, this issue, 1161–1173.

Yernool, D., Boudker, O., Folta-Stogniew, E., and Gouaux, E. (2003). Trimeric subunit stoichiometry of the glutamate transporters from Bacillus caldotenax and Bacillus stearothermophilus. Biochemistry *42*, 12981–12988.

Accession Numbers

The structures described herein have been deposited in the Protein Data Bank with ID codes 2HMT, 2HMU, and 2HMV for the diamond conformation; 2HMS for the rectangle; and 2HMW for the square.